Journal of Sound and Vibration (2003) **259**(5), 1109–1129
doi:10.1006/jsvi.2002.5118, available online at http://www.idealibrary.com on IDEAL®

POWER FLOW ANALYSIS OF REINFORCED BEAM–PLATE COUPLED STRUCTURES

SEONG-HOON SEO AND SUK-YOON HONG

Department of Naval Architecture and Ocean Engineering, Seoul National University, Seoul 151-742, *South Korea. E-mails: syhong@gong.snu.ac.kr*

AND

HYUN-GWON KIL

Department of Mechanical Engineering, The University of Suwon, Suwon 445-743, *South Korea*

(*Received* 15 *May* 2001, *and in final form* 16 *April* 2002)

A power flow analysis method was developed to predict the vibrational responses of reinforced beam–plate coupled structures in frequencies ranging from medium to high. This analysis method was successfully applied to simply supported rectangular plates reinforced with multi-parallel beams by utilizing the power flow coupling relationships at the beam–plate junctions and the zero intensity conditions at the plate edges. Through numerical simulations, the power flow energy density and intensity fields of two different plates, consisting of single beam and eight beams, were compared with those of classical displacement solutions, and they show good agreement in terms of the global decay and the attenuation patterns of the energy density.

1. INTRODUCTION

Many engineering structures are designed as plate components with reinforcing beams to provide effective strength and resistance to vibrational motions. The reinforcing beam is the structural element of greatest practical importance in ship superstructures, bridge decks, ribbed floors, aircraft and space structures. At low-frequency ranges, the vibrational response of these structures may be analyzed with regards to structural deformations by conventional methods such as the finite element method (FEM). However, at high frequency or for broadband analysis, an alternative approach is required because conventional methods demand excessive computation time.

Recent investigations have considered power flow analysis (PFA), which is analogous to the steady state heat flow model, as a possible alternative approach. In this method, the primary response variable is the vibration energy density of the structure and the secondary response variable is the vibration intensity vector which is proportional to the gradient of the energy density. For longitudinal vibration in rods and transverse flexural vibration of beams, Wohlever and Bernhard [1] have found that time- and space-averaged farfield intensity is proportional to the gradient of total energy density, and have derived approximate energy governing equations. Bouthier and Bernhard [2] also have developed energy governing equations for flexural wave in plates and applied it to a single plate. Cho

0022-460X/02/$35.00

[3] has utilized PFA to predict the vibration response of coupled plate structures by applying the power flow coupling relationships to the coupled plate junctions. In this study, the diffused power transmission and reflection concept is used in semi-infinite coupled plates because the frequency-averaged vibration responses of finite structures are close to those of similar types of infinite structures [4]. Park [5, 6] has derived completely energy governing equations for in-plane waves such as longitudinal wave and shear wave in plates. Seo [7] has developed 3d.o.f. finite element formulations of energy governing equations for flexural, longitudinal, and shear waves in plates.

Up to now, most PFA investigations have concentrated on developing power flow models of a single structure or coupled structures consisting of similar types of elements. The main purpose of this study is to develop an adequate PFA method for application to reinforced beam–plate coupled structures and consequently to prove the efficacy of the PFA method relative to the classical method. Reinforced beam–plate structures are modelled on simply supported plates with uniformly parallel multi-reinforcing beams. For rigorous consideration of the discrete nature of the beams, the energy density satisfies the energy governing equations of the plates in their domains and the power flow coupling relationships are applied to the plate–beam junctions.

In the next section, power transmission and reflection coefficients at the plate–beam junctions are discussed. In section 3, power flow analysis solutions of the beam-reinforced plates are discussed, and in section 4, the power flow analysis solutions and displacement solutions are compared for several different conditions.

2. WAVE TRANSMISSION ANALYSIS OF BEAM-REINFORCED PLATES

Cremer and Heckl [8] have established the transmission and reflection characteristics of various structural junctions. For the reinforced plate part, their study assumed that a thin and rectangular beam is symmetrically connected with co-planar plates, and simple boundary conditions were applied. Therefore, the displacements at both sides of the plate–beam junction were same. Langley and Heron [9] have investigated power transmission coefficients for the more general types of structural junctions which consist of an arbitrary number of plates coupled through a beam of arbitrary shape. In this section, the wave transmission approach is applied to the structural junctions between plates and a beam.

Figure 1(a) shows the cross-section of a semi-infinite rectangular beam joined, along its length, to N semi-infinite plates of different materials and geometrical properties. The centroid line of the beam is the y_b axis of its co-ordinate system (x_b, y_b, z_b) and is the same in terms of its shear axis due to the symmetry cross-section. The plate m, one of i, $1, 2, \ldots, N-1$ is joined at J_m at angle θ_m from x_b and follows the local co-ordinate system (x_m, y_m, z_m). Figure 1(b) shows the plane of plate I from which an incident wave strikes the reinforcing beam at angle ϕ_m from normal to the junction line.

When a flexural wave of amplitude $\overline{A_f}$, or a longitudinal wave of amplitude $\overline{A_l}$, or a shear wave of amplitude $\overline{A_s}$ is incident as a plane wave form propagating in the plate i, transmitted or reflected wave is generated in each semi-infinite plate. The x, y, and z directional displacements (u_i, v_i, and w_i) of the incident plate i in its local co-ordinate can be represented as follows:

$$u_i(x,y) = -\frac{k_{lxi}}{k_{li}}\overline{A_l}\mathrm{e}^{\mathrm{j}k_{lxi}x-\mathrm{j}k_y y} - \frac{k_y}{k_{si}}\overline{A_s}\,\mathrm{e}^{\mathrm{j}k_{sxi}x-\mathrm{j}k_y y} + \frac{k_{lxi}}{k_{li}}P_{li}\mathrm{e}^{-\mathrm{j}k_{lxi}x-\mathrm{j}k_y y} - \frac{k_y}{k_{si}}Q_{si}\,\mathrm{e}^{-\mathrm{j}k_{sxi}x-\mathrm{j}k_y y}, \quad (1)$$

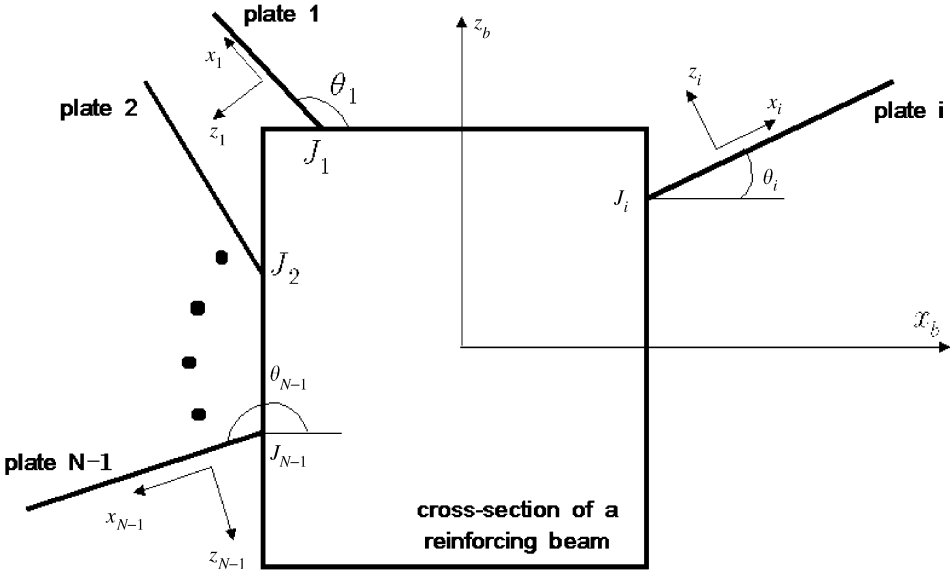

(a)

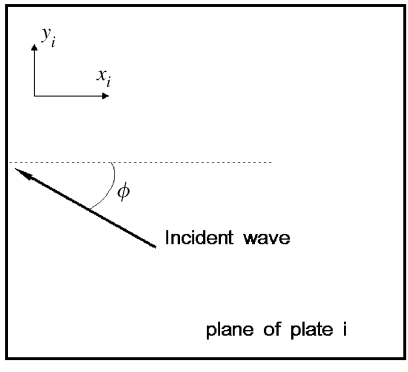

(b)

Figure 1. (a) Cross-section of N plates joined to a rectangular beam and a co-ordinate system for the plates and the beam. (b) Plane of an incident plate.

$$v_i(x,y) = -\frac{k_y}{k_{li}}\overline{A_l}\mathrm{e}^{\mathrm{j}k_{lxi}x-\mathrm{j}k_y y} - \frac{k_{sxi}}{k_{si}}\overline{A_s}\mathrm{e}^{\mathrm{j}k_{sxi}x-\mathrm{j}k_y y} + \frac{k_y}{k_{li}}P_{li}\mathrm{e}^{-\mathrm{j}k_{lxi}x-\mathrm{j}k_y y} + \frac{k_{sxi}}{k_{si}}Q_{si}\mathrm{e}^{-\mathrm{j}k_{sxi}x-\mathrm{j}k_y y}, \tag{2}$$

$$w_i(x,y) = \overline{A_f}\mathrm{e}^{\mathrm{j}k_{fxi}x-\mathrm{j}k_y y} + B_i\mathrm{e}^{-\mathrm{j}k_{fxi}x-\mathrm{j}k_y y} + C_i\mathrm{e}^{-\sqrt{k_{fi}^2+k_y^2}x-\mathrm{j}k_y y}. \tag{3}$$

In equations (1) and (2), the first and second terms are the incident longitudinal and shear waves, respectively, and the third and fourth are the reflected longitudinal and shear waves respectively. In equation (3), the first term is the incident flexural propagating wave, the second is the flexural reflected propagating wave, and the third is the reflected decaying nearfield wave. The terms k_{fm}, k_{lm} and k_{sm} are the flexural, longitudinal and shear wavenumbers of the plate m, respectively, and are related to the following equations:

$$k_{fm} = (\omega^2 \rho_m h_m / D_m)^{1/4}, \tag{4}$$

$$k_{lm} = \omega / (E_m / \rho_m (1 - \upsilon_m^2))^{1/2}, \tag{5}$$

$$k_{sm} = \omega / (G_m / \rho_m)^{1/2}, \tag{6}$$

where ω, ρ, h, E, and υ are the frequency of the incident wave, the material density, the thickness, Young's modulus and the Possion ratio respectively. $D = Eh^3/(1-\upsilon^2)$ and $G = E/2(1+\upsilon)$ are the flexural stiffness and shear modulus of a plate. The term k_y is the y directional wavenumber of the incident wave expressed with the incident wavenumber k as

$$k_y = k \sin \phi \tag{7}$$

and all the waves of the plates and the beam produced by the incident wave share the factor $e^{-jk_y y}$, since they share the same wave motion along the junctions. The terms k_{fxm}, k_{lxm} and k_{sxm} are the x directional wavenumbers of k_{fk}, k_{lk}, and k_{sk}, which can be defined as follows for the purpose of numerical convenience:

$$k_{pxm} = \begin{cases} k_i \sqrt{\alpha_{pm}^2 - \sin^2 \phi}, & \alpha_{pm} > \sin \phi, \\ -jk_i \sqrt{\sin^2 \phi - \alpha_{pm}^2} & \alpha_{pm} < \sin \phi. \end{cases} \tag{8}$$

Here, the subscript p indicates one of the wave types among the flexural(f), longitudinal (l) and shear (s) waves. The term α_{pm} is wavenumber ratio of the p type wave at the transmitted or reflected plate m to the incident wavenumber. If $\alpha_{pm} > \sin \phi$, k_{pxm} becomes real and the p type wave at the transmitted or reflected plate m represents a propagating wave. Otherwise, k_{pxm} is a purely imaginary number and the p type wave at the plate m represents a decaying wave.

The x, y, and z directional displacements (u_t, v_t, and w_t) in the transmitted plate can be represented as follows:

$$u_t(x,y) = \frac{k_{lxt}}{k_{lt}} P_{lt} e^{-jk_{lxt}x - jk_y y} - \frac{k_y}{k_{st}} Q_{st} e^{-jk_{sxt}x - jk_y y}, \tag{9}$$

$$v_t(x,y) = \frac{k_y}{k_{lt}} P_{lt} e^{-jk_{lxt}x - jk_y y} + \frac{k_{sxt}}{k_{st}} Q_{st} e^{-jk_{sxt}x - jk_y y}, \tag{10}$$

$$w_t(x,y) = B_t e^{-jk_{fxt}x - jk_y y} + C_t e^{-\sqrt{k_{ft}^2 + k_y^2}x - jk_y y}. \tag{11}$$

In equations (9) and (10), the first and second terms are the transmitted longitudinal and shear waves respectively. In equation (11), the first term is the flexural transmitted propagating wave and the second represents the transmitted decaying nearfield wave.

The displacements of the reinforcing beam in the beam co-ordinate system can be represented as

$$w_{bx}(y) = F_x e^{-jk_y y}, \tag{12}$$

$$w_{bz}(y) = F_z e^{-jk_y y}, \tag{13}$$

$$u_b(y) = L_b e^{-jk_y y}, \tag{14}$$

$$\theta_b(y) = T_b e^{-jk_y y}, \tag{15}$$

where w_{bx} and w_{bz} are the x and z directional transverse waves, respectively, and where u_b is a longitudinal wave and θ_b is a torsional wave of the beam.

In equations (1)–(3) and (9)–(15), the $4N$ complex amplitudes (P_{lm}, Q_{sm}, B_m and C_m) of the plates and the 4 complex amplitudes (F_x, F_z, L_b and T_b) of the beam are determined from the following $4N + 4$ equilibrium conditions at the junctions. The $3N$ among the $4N + 4$ conditions impose continuity of displacement between the beam and plates in the three directions of the beam as follows:

$$\theta_b z_{Jm} + w_{bx} = u_m \cos\theta_m - w_m \sin\theta_m, \quad m = I, \quad 1, 2, \ldots, N-1, \tag{16}$$

$$u_b = v_m, \quad m = I, \quad 1, 2, \ldots, N-1, \tag{17}$$

$$-\theta_b x_{Jm} + w_{bx} = u_m \sin\theta_m + w_m \cos\theta_m, \quad m = I, \quad 1, 2, \ldots, N-1, \tag{18}$$

where (x_{Jm}, z_{Jm}) indicates the co-ordinates of the junctions J_m between the beam and m_{th} plate. The N conditions impose continuity of slope between the beam and plates in the y direction of the beam as follows:

$$\theta_b = -\partial w_m / \partial x, \quad m = I, \quad 1, 2, \ldots, N-1. \tag{19}$$

The remaining three conditions impose force equilibrium in the three directions of the beam as follows:

$$\sum_{k=1}^{N} \{N_{xx}^k \cos\theta_k - Q_{xz}^k \sin\theta_k\} + \frac{\partial V_{yx}}{\partial y} = m_b \frac{\partial^2 w_{bx}}{\partial t^2}, \tag{20}$$

$$\sum_{k=1}^{N} N_{xy}^k + \frac{\partial F_{yy}}{\partial y} = m_b \frac{\partial^2 u_{by}}{\partial t^2}, \tag{21}$$

$$\sum_{k=1}^{N} \{N_{xx}^k \sin\theta_k + Q_{xz}^k \cos\theta_k\} + \frac{\partial V_{yz}}{\partial y} = m_b \frac{\partial^2 w_{bz}}{\partial t^2}, \tag{22}$$

where N_{xx}, N_{xy} and Q_{xz} are the extensional force, shear force of in-plane motion and effective shear force of bending motion per unit plate length, respectively, and can be written as

$$N_{xx} = Eh\left(\frac{\partial u}{\partial x} + \upsilon \frac{\partial v}{\partial y}\right), \tag{23}$$

$$N_{xy} = Gh\left(\frac{\partial u}{\partial y} + \frac{\partial v}{\partial x}\right), \tag{24}$$

$$Q_{xz} = -D\left(\frac{\partial^3 w}{\partial x^3} + (2 - \upsilon)\frac{\partial^3 w}{\partial x \partial y^2}\right), \tag{25}$$

The term m_b is the mass per unit beam length and V_{yx}, V_{yz} and F_{yy} are the x and z directional shear forces and the axial force of the beam respectively. They can be written with the moments of inertia I_x, I_z for the x and z axes and the cross-sectional area S_b as

$$V_{yx} = -EI_z \frac{\partial^3 w_{bx}}{\partial y^3}, \tag{26}$$

$$V_{yz} = -EI_x \frac{\partial^3 w_{bz}}{\partial y^3}, \tag{27}$$

$$F_{yy} = ES_b \frac{\partial^3 u}{\partial y}. \tag{28}$$

The last condition imposes the moment equilibrium in the y direction as

$$\sum_{k=1}^{N} \{M_{xx}^k + N_{xx}^k (y_{Jk} \cos\theta_k - x_{Jk} \sin\theta_k) + V_{xz}^k (-y_{Jk} \sin\theta_k - x_{Jk} \cos\theta_k)\} + \frac{\partial M_t}{\partial y} = J_b \frac{\partial^2 \theta_b}{\partial t^2}, \tag{29}$$

where J_{by} is the mass moment of inertia per unit beam length. And the bending moment per unit plate length M_{xx} and the torque of the beam M_t can be written as

$$M_{xx} = -D\left(\frac{\partial^2 w}{\partial x^2} + \upsilon \frac{\partial^2 w}{\partial y^2},\right) \tag{30}$$

$$M_t = T_b \frac{\partial \theta_b}{\partial y}, \tag{31}$$

where T_b is the torsional stiffness of the beam.

By substituting the displacement equations (1)–(3) and (9)–(15), into the equilibrium equations (16)–(22) and (29), the equilibrium conditions at the joint are expressed in terms of the amplitudes of the plates and beam. Then the equilibrium equations are solved simultaneously for the reflected and transmitted complex amplitudes in terms of the incident amplitude for each incident wave type.

In the incident plate i, the time-averaged power inputs in the x direction for each incident wave type are obtained as

$$\langle P_f \rangle_i = Dk_{fi}^3 \omega \left|\overline{A_f}\right|^2 \cos\phi, \tag{32}$$

$$\langle P_l \rangle_i = 1/2 Ehk_{li} \omega \left|\overline{A_l}\right|^2 \cos\phi, \tag{33}$$

$$\langle P_s \rangle_i = 1/2 Ghk_{si} \omega \left|\overline{A_s}\right|^2 \cos\phi. \tag{34}$$

The time-averaged power transmitted or reflected by the plate m in the x direction for each incident wave type can be written as

$$\langle P_f \rangle_m = \mathrm{Re}\left[D_m k_{fm}^2 \omega |B_m|^2 k_{fxm}\right], \qquad \langle P_l \rangle_m = \mathrm{Re}\left[1/2 E_m h_m k_{lxm} \omega |P_{lm}|^2\right], \tag{35, 36}$$

$$\langle P_s \rangle_m = \mathrm{Re}\left[1/2 G_m h_m k_{sxm} \omega |Q_{sm}|^2\right], \tag{37}$$

Here, the transmitted or reflected power will be zero if a decaying wave is transmitted or reflected by the incident wave, since the x directional wavenumber is a pure imaginary number.

When the p type incident wave in plate i is transmitted or reflected into the q type wave in plate m or plate i, the diffused power transmitted coefficients $\langle \tau_{pq} \rangle_{im}$ and reflected coefficients $\langle \gamma_{pq} \rangle_{ii}$ can be expressed as

$$\langle \tau_{pq} \rangle_{im} = \frac{\int_{-\pi/2}^{\pi/2} \langle P_q \rangle_m \, \mathrm{d}\theta}{\int_{-\pi/2}^{\pi/2} \langle P_p \rangle_i \, \mathrm{d}\theta}, \qquad \langle \gamma_{pq} \rangle_{ii} = \frac{\int_{-\pi/2}^{\pi/2} \langle P_q \rangle_i \, \mathrm{d}\theta}{\int_{-\pi/2}^{\pi/2} \langle P_p \rangle_i \, \mathrm{d}\theta}. \tag{38, 39}$$

These diffused coefficients are used in power flow relationships for the reinforced beam–plate coupled structures.

3. POWER FLOW ANAYSIS OF SIMPLY SUPPORTED RECTANGULAR PLATES WITH MULTI-REINFORCING BEAMS

Consider the $N+2$ simply supported rectangular plates to which N rectangular cross-sectioned reinforcing beams are joined symmetrically as shown in Figure 2. The plate between beam p and beam $p+1$ is excited by a vertical point loading and is divided into two parts by the loading line paralleled with the beam.

The power flow analysis model to describe the vibration of the plates can be assumed as shown in Figure 3 using the zero intensity boundary conditions at the plate edges, the power balance relationship at the excitation location and the power flow coupling relationships at the plate–beam junctions. If the beam is assumed to have no mechanical

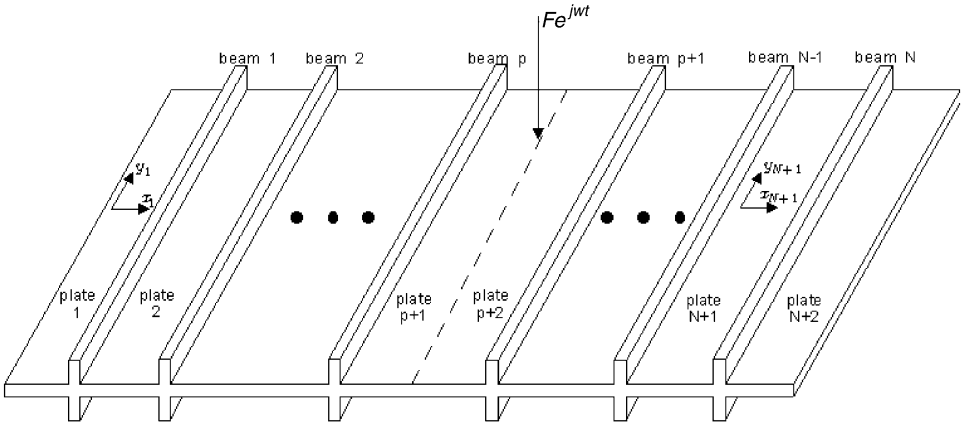

Figure 2. Rectangular plate structures with N reinforcing beams driven by point loading. All edges are simply supported.

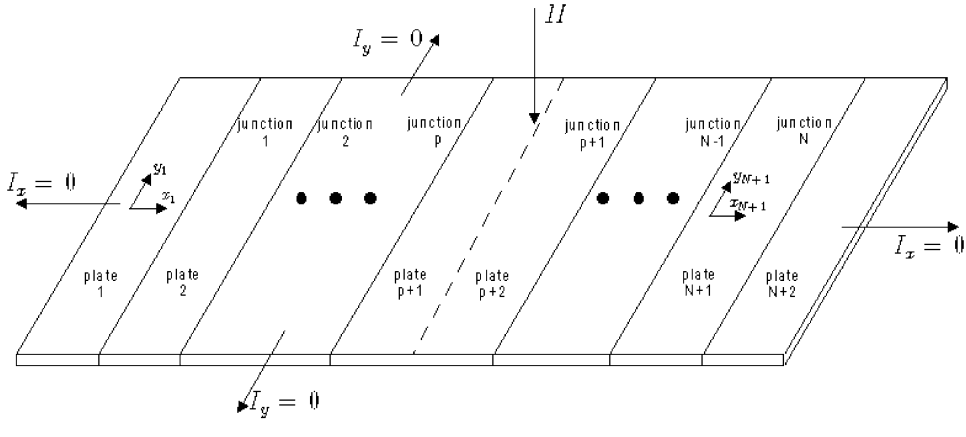

Figure 3. Power flow model equivalent to the structures shown in Figure 2.

internal loss factor and if the in-plane waves energy density of the plates is ignored, only the flexural wave energy density of the plates is considered. The energy governing equation for the flexural waves in homogeneous plates is known to be

$$-\frac{c_g^2}{\eta\omega}\left(\frac{\partial^2}{\partial x^2}+\frac{\partial^2}{\partial y^2}\right)\langle \mathrm{e}\rangle + \eta\omega\langle \mathrm{e}\rangle = 0, \tag{40}$$

where c_g is the group velocity of the flexural waves, η is the internal loss factor and $\langle e\rangle$ is the flexural wave energy density. The time-averaged farfield intensity for the flexural waves in the plate can be expressed as

$$\langle \vec{I}\rangle = -\frac{c_g^2}{\eta\omega}\left(\frac{\partial}{\partial x}\vec{x}+\frac{\partial}{\partial y}\vec{y}\right)\langle \mathrm{e}\rangle. \tag{41}$$

Since the boundary condition for each rectangular plate is such that the intensity at any two opposite edges ($y_k = 0$ and $y_k = L_y$) is zero, the solution of equation (41) can be expressed by the Lévy Method with the Fourier cosine series

$$\langle e\rangle(x,y) = \sum_{m=0}^{\infty} Y_m(x)\cos\frac{m\pi y}{L_y}, \tag{42}$$

where $Y_m(x)$ is yet to be determined and must satisfy the appropriate boundary conditions at the other edges ($x_k = 0$ and $x_k = L_{xk}$). Substituting equation (42) into equation (40) yields:

$$Y_m''(x) - \left(\left(\frac{m\pi}{L_y}\right)^2 + \left(\frac{\eta\omega}{c_g}\right)^2\right) Y_m(x) = 0. \tag{43}$$

The general solution of equation (43) is written as

$$Y_m(x) = A\mathrm{e}^{\Phi_m x} + B\mathrm{e}^{-\Phi_m x} \tag{44}$$

where A and B are arbitrary constants and Φ_m is defined as

$$\Phi_m = \left(\frac{m\pi}{L_y}\right)^2 + \left(\frac{\eta\omega}{c_g}\right)^2. \tag{45}$$

By substituting equation (44) into equation (42), the energy density of each plate yields

$$\langle e\rangle_k(x,y) = \sum_{m=0}^{\infty}\left(A_k\mathrm{e}^{\Phi_{mk}x} + B_k\mathrm{e}^{-\Phi_{mk}x}\right)\cos\frac{m\pi y}{L_y},\quad k = 1,2,\ldots,N+2 \tag{46}$$

where the subscript k is the index of the plates. On the right-hand side of equation (46), the first and second terms can be expressed as $\langle e_x\rangle_k^-$ and $\langle e_x\rangle_k^+$, respectively, by the direction of the travelling flexural waves. By substituting equation (46) into equation (41), the intensity components can written as

$$\langle \mathbf{I}_x\rangle_k(x,y) = -\frac{c_g^2}{\eta\omega}\sum_{m=0}^{\infty}\Phi_{mk}\left(A_k\mathrm{e}^{\Phi_{mk}x} - B_k\mathrm{e}^{-\Phi_{mk}x}\right)\cos\frac{m\pi y}{L_y}, \tag{47}$$

$$\langle \mathbf{I}_y\rangle_k(x,y) = \frac{c_g^2}{\eta\omega}\sum_{m=0}^{\infty}\frac{m\pi}{L_y}\left(A_k\mathrm{e}^{\Phi_{mk}x} + B_k\mathrm{e}^{-\Phi_{mk}x}\right)\sin\frac{m\pi y}{L_y} \tag{48}$$

On the right-hand side of equation (47), the first and second terms can be expressed as $\langle \mathbf{I}_x\rangle_k^-$ and $\langle \mathbf{I}_x\rangle_k^+$, respectively, by the direction of the travelling flexural waves.

$A_1, A_2, \ldots, A_{N+1}$ and $B_1, B_2, \ldots, B_{N+1}$ are determined by $2\times(N+1)$ appropriate boundary conditions. Two of the boundary conditions applied are zero intensity in the x

direction at $x_1 = 0$ and $x_{N+2} = L_{xN+2}$, and subsequently with equation (47), the following relations are obtained:

$$\sum_{m=0}^{\infty}(A_k - B_k) = 0, \qquad \sum_{m=0}^{\infty}\left(A_k e^{\Phi_{mN+2}L_{xN+2}} - B_k e^{-\Phi_{mN+2}L_{xN+2}}\right) = 0. \tag{49, 50}$$

Two of the boundary conditions are from the relationship between the energy and power balance at the line $x_p = L_{xp}$, and hence the continuity of the energy density $\langle e\rangle_p(L_{xp}, y) = \langle e\rangle_{p+1}(0, y)$ yields:

$$\sum_{m=0}^{\infty}\left(A_p e^{\Phi_{mp}L_{xp}} + B_p e^{-\Phi_{mp}L_{xp}}\right) = \sum_{m=0}^{\infty}(A_{p+1} + B_{p+1}). \tag{51}$$

Also, the power balance relationship is

$$\langle \mathbf{I}_x\rangle_{p+1}(0, y) = \langle \mathbf{I}_x\rangle_p(L_{xp}, y) + \Pi\delta(y - y_F), \tag{52}$$

where Π is the input power that can be expressed using the Fourier cosine series as

$$\Pi\delta(y - y_F) = \sum_{m=0}^{\infty}\frac{\Lambda_m}{L_y}\Pi\cos\frac{m\pi y_F}{L_y}\cos\frac{m\pi y}{L_y}. \tag{53}$$

Here, Λ_m has the constant value of 1 at $m = 0$ or 2 at $m \neq 0$. Substituting equations (48)–(53) into equation (52) yields

$$\sum_{m=0}^{\infty}\Phi_m(A_{p+1} - B_{p+1}) = \sum_{m=0}^{\infty}\Phi_m\left(A_p e^{\Phi_{mp}L_{xp}} - B_p e^{-\Phi_{mp}L_{xp}}\right) + \sum_{m=0}^{\infty}\frac{\Lambda_m}{L_y}\Pi\cos\frac{m\pi y_F}{L_y}. \tag{54}$$

The rest boundary conditions result from the power flow coupling relationships of each plate–beam junction as follows for $k = 1, 2, \ldots, N + 1$ except p:

$$\langle \mathbf{I}_x\rangle_{k+1}^{+}(0, y) = \langle \tau_{ff}\rangle_{kk+1}\langle \mathbf{I}_x\rangle_k^{+}(L_{xk}, y) - \langle \gamma_{ff}\rangle_{k+1k+1}\langle \mathbf{I}_x\rangle_{k+1}^{-}(0, y), \tag{55}$$

$$-\langle \mathbf{I}_x\rangle_k^{-}(L_{xk}, y) = \langle \gamma_{ff}\rangle_{kk}\langle \mathbf{I}_x\rangle_k^{+}(L_{xk}, y) - \langle \tau_{ff}\rangle_{k+1k}\langle \mathbf{I}_x\rangle_{k+1}^{-}(0, y), \tag{56}$$

where $\langle \tau_{ff}\rangle_{ij}$ is the diffused flexural power transmission coefficient in plate j due to the incident flexural wave in plate i, and where $\langle \gamma_{ff}\rangle_{ii}$ is the diffused flexural power reflection coefficient in plate i due to the incident flexural wave in plate i, as shown in section 2.

Substituting equation (47) into equations (55) and (56) yields for$k = 1, 2, \cdots, N + 1$ except p:

$$\frac{c_{gk+1}^2}{\eta\omega}\sum_{m=0}^{\infty}\Phi_{mk+1}B_{k+1} = \langle \tau_{ff}\rangle_{kk+1}\frac{c_{gk}^2}{\eta\omega}\sum_{m=0}^{\infty}\Phi_{mk}B_k e^{-\Phi_{mk}L_{xk}} + \langle \gamma_{ff}\rangle_{k+1k+1}\frac{c_{gk+1}^2}{\eta\omega}\sum_{m=0}^{\infty}\Phi_{mk+1}A_k, \tag{57}$$

$$\frac{c_{gk}^2}{\eta\omega}\sum_{m=0}^{\infty}\Phi_{mk}A_k e^{\Phi_{mk}L_{yk}} = \langle \gamma_{ff}\rangle_{kk}\frac{c_{gk}^2}{\eta\omega}\sum_{m=0}^{\infty}\Phi_{mk}B_k e^{-\Phi_{mk}L_{yk}} + \langle \tau_{ff}\rangle_{k+1k}\frac{c_{gk+1}^2}{\eta\omega}\sum_{m=0}^{\infty}\Phi_{mk+1}A_{k+1}. \tag{58}$$

The terms A_k and B_k of equations (49)–(51), and (54) and (57) and (58) can be calculated numerically for each mode m. By substituting the computed A_k and B_k into equations (46)–(48), the power flow solutions of the plates are obtained for energy density and intensity.

4. NUMERICAL SIMULATION

In this section, several numerical simulations for the two different models are performed and compared with the classical energy density and intensity calculated from displacement

solutions in order to demonstrate the reliability of the derived power flow equation and the solutions presented in section 3. The decibel scales of the energy density and intensity referenced to $10^{-12}\,\mathrm{J/m^2}$ and $10^{-12}\,\mathrm{W/m^2}$ are used in all figures of the simulation results. The displacement solutions for the structures shown in Figure 2 are obtained using the Lévy method generally used for power flow solutions, by applying the end conditions. Here, the plate edges are simply supported, and the boundary conditions with the displacement continuity and force/moment equilibrium at plate–beam junctions are used as previously described in section 2. For the band analysis the frequency band energy

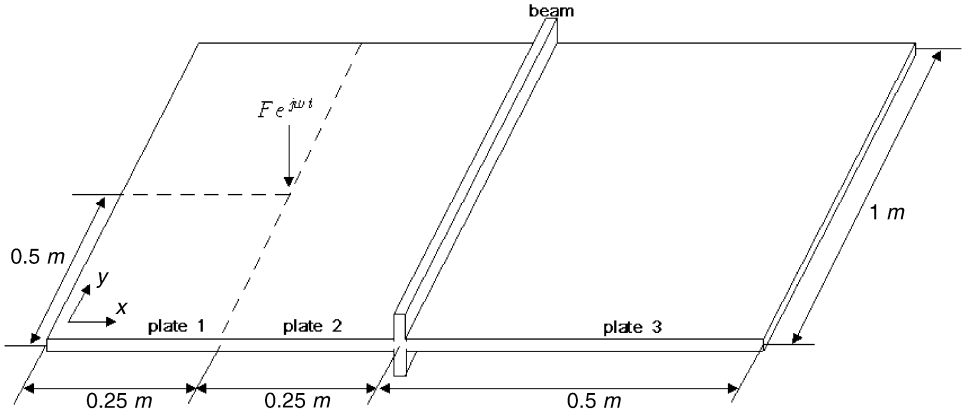

Figure 4. Reinforced plate with single beam. All edges are simply supported.

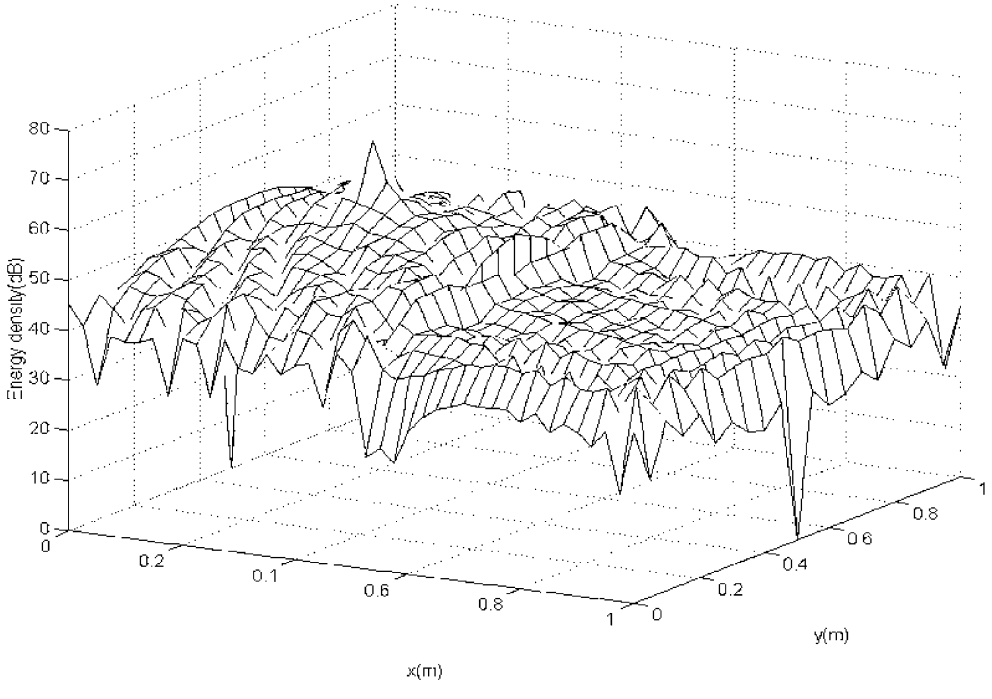

Figure 5. Energy density distribution of the displacement solutions when $f_c = 5000\,\mathrm{Hz}$ and $\eta = 0{\cdot}1$.

density is calculated by numerically integrating the energy density over the band using the trapezoidal rule [10, 11]. The spectral contents of the excitation force are assumed to be flat between the lower cut-off frequency f_1 and the upper cut-off frequency f_2.

The power flow solutions are solved only at the center frequency f_c. In the frequency averages, the power input given to the finite structures at the excitation location can be deduced approximately using the exciting force Fe^{jwt} and the mobility M_{in} derived from a similar type of infinite structures with the equation:

$$\Pi_{in} = \tfrac{1}{2}|F|^2 \mathrm{Re}\{M_{in}\} \tag{59}$$

as discussed by Cremer and Heckl [9].

For the first model, the $1\,\mathrm{m} \times 1\,\mathrm{m} \times 5\,\mathrm{mm}\,(L \times B \times H)$ steel plate structures reinforced with a $5\,\mathrm{mm} \times 50\,\mathrm{mm}\,(B \times H)$ steel beam are selected as seen in Figure 4. The structures are driven by point loading of magnitude $F = 1N$ at the co-ordinates, 0·25, 0·5(0·25, 0·5). Figures 5 and 6 show the energy density distributions of the displacement solutions and power flow solutions, respectively, for the 1/3 octave band with $f_c = 5000\,\mathrm{Hz}$ and $\eta = 0{\cdot}1$. As expected, the energy density of the displacement solutions decreases universally with increasing distance from the excitation location and fluctuates locally in space, especially near the edges of the plates and the junction. The energy density of the power flow solutions shown in Figure 6 varies smoothly in space without any fluctuation and has a discontinuity line at the plate–beam junction. Figure 7 shows the compared result of the energy density distributions from Figures 5 and 6 along the line $y = 0{\cdot}5$. The displacement solutions fluctuate in the vicinity of the smoothed result of the power flow solutions. Figures 8 and 9 show that the intensity fields of the displacement solutions and power flow solutions respectively. The intensity field in Figure 5 appears to be far more intricate than that in Figure 6, but both are similar in terms of power flow tendency.

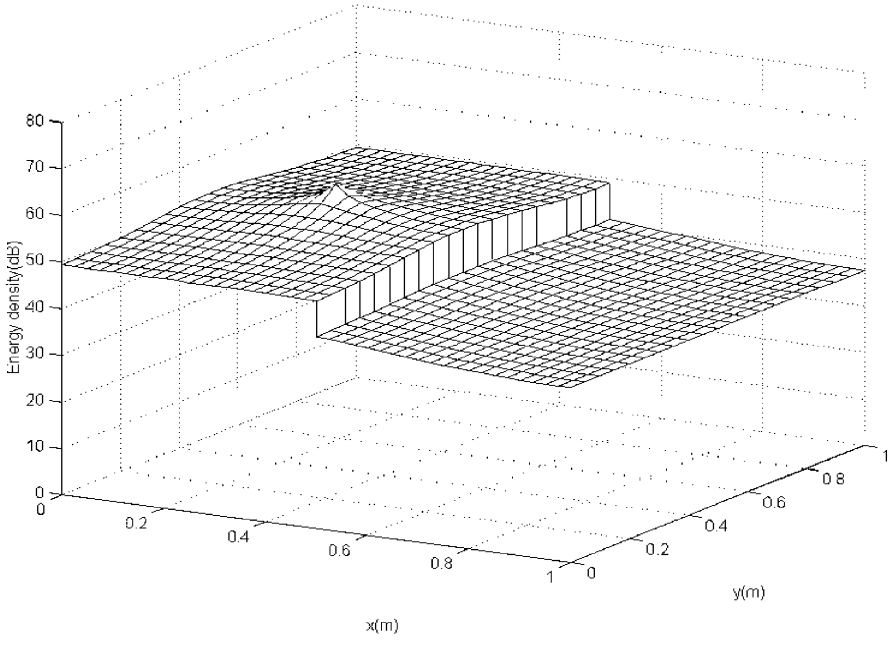

Figure 6. Energy density distribution of the power flow solutions when $f_c = 5000\,\mathrm{Hz}$ and $\eta = 0{\cdot}1$.

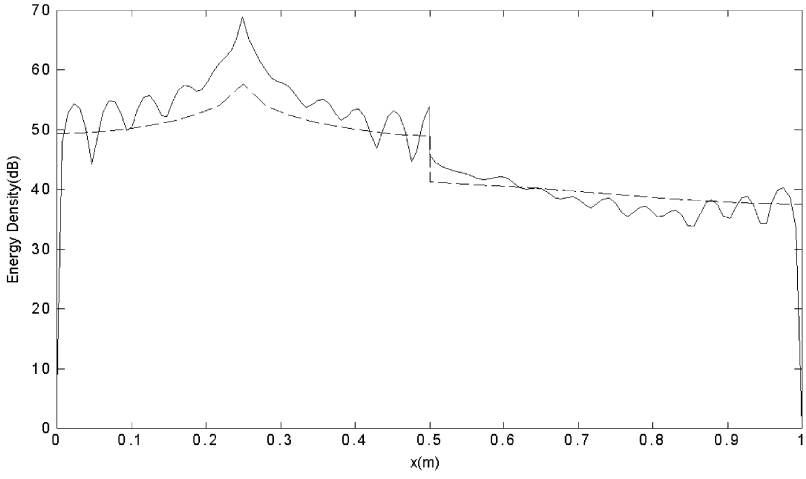

Figure 7. Energy density distribution comparison along the line $y = 0.5$ when $f_c = 5000$ Hz and $\eta = 0{\cdot}1$: ——, displacement solution; – – – –, power flow solution.

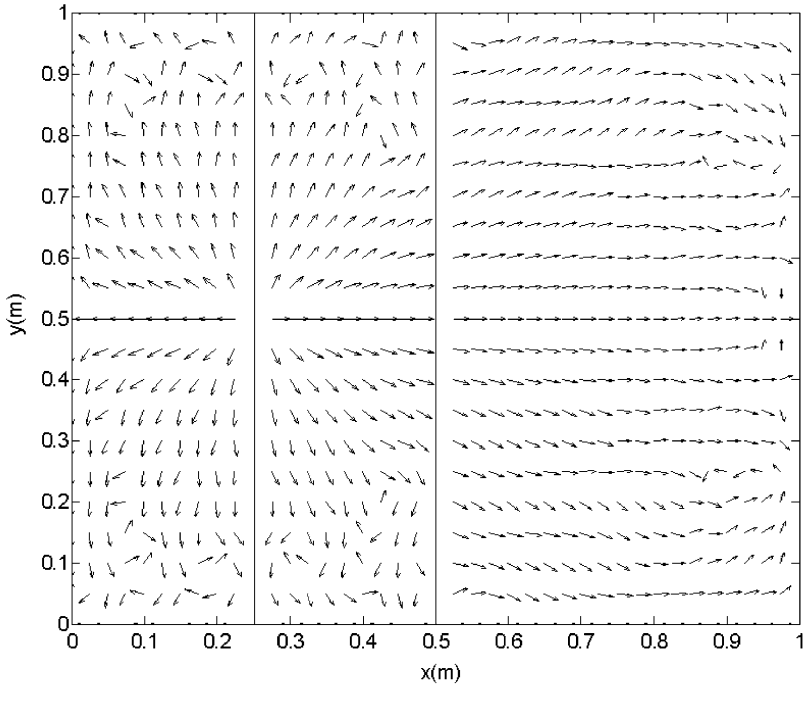

Figure 8. Intensity field of the displacement solutions when $f_c = 5000$ Hz and $\eta = 0{\cdot}1$.

For the following simulations, the exciting frequency band and/or internal loss factor are changed. Figure 10 compares the results of the energy density distributions of the displacement solutions and power flow solutions along the line $y = 0{\cdot}5$ for the 1/3 octave band with $f_c = 1000$ Hz, with the other parameters used in Figures 5–9 remaining

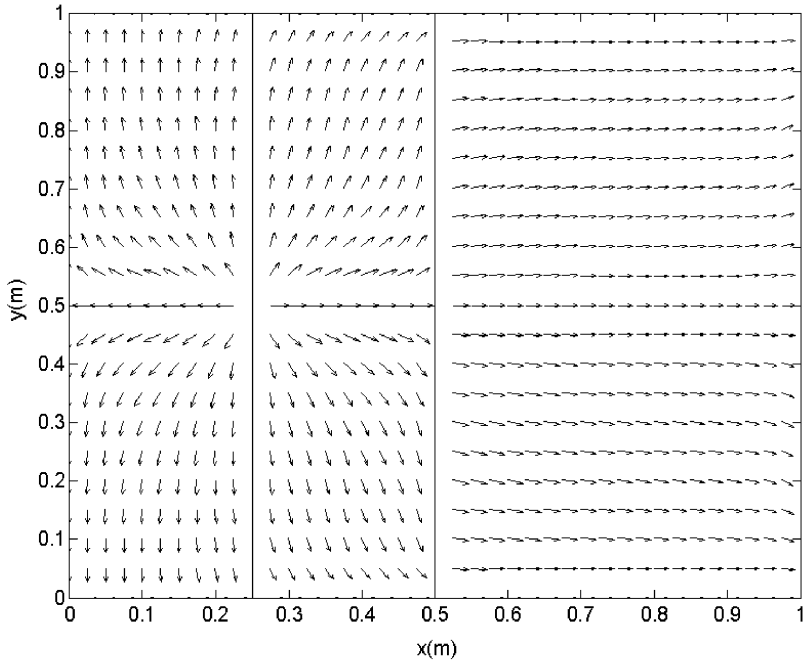

Figure 9. Intensity field of the power flow solutions when $f_c = 5000$ Hz and $\eta = 0{\cdot}1$.

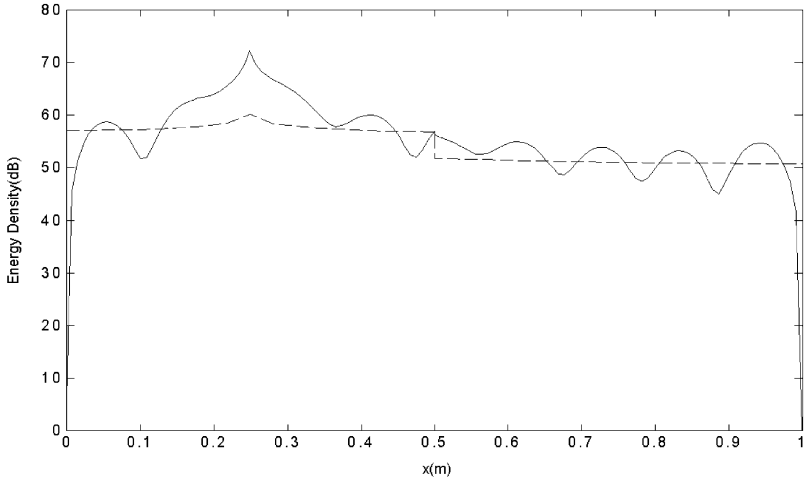

Figure 10. Energy density distribution comparison along the line $y = 0.5$ when $f_c = 1000$ Hz and $\eta = 0{\cdot}1$: ——, displacement solution; – – – – –, power flow solution.

unchanged. This analysis method is repeated for the results presented in Figure 11 but with a different internal loss factor of 0·01. As shown in many previous studies on power flow analysis [1–3, 5–7, 10], the comparison of Figures 7, 10 and 11 confirms that the spatial energy density exhibits a more global decay as the frequency or internal loss factor increases.

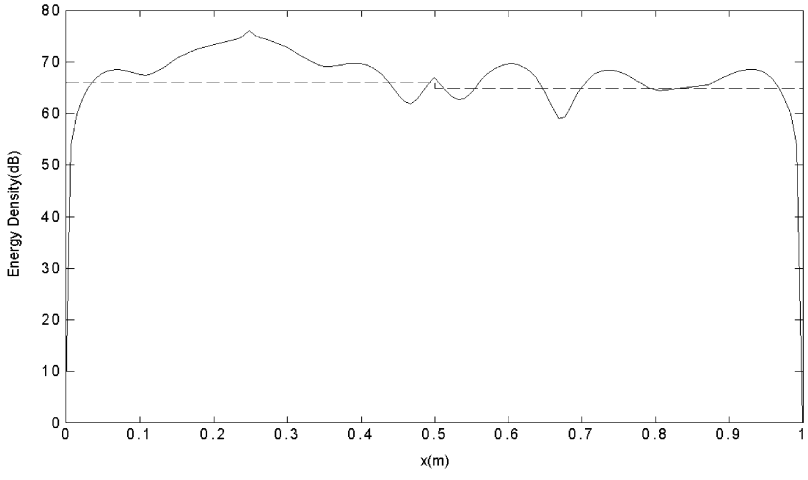

Figure 11. Energy density distribution comparison along the line $y = 0.5$ when $f_c = 1000$ Hz and $\eta = 0{\cdot}01$: ——, displacement solution; – – – – –, power flow solution.

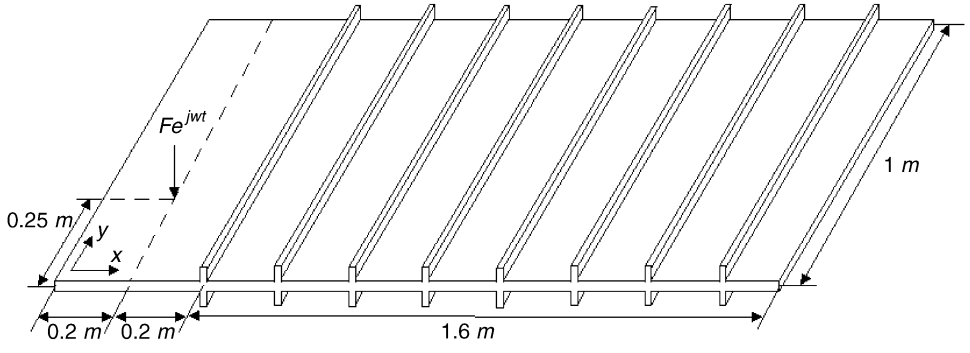

Figure 12. Reinforced plate with 8 beams. All edges are simply supported.

For the second model, the simple supported plates with multi-beams are chosen as shown in Figure 12. The 8 steel beams separated by a uniform 0.2 m space with the cross-section of $5\,\text{mm} \times 20\,\text{mm}$ $(B \times H)$, are joined symmetrically to $2\,\text{m} \times 1\,\text{m} \times 5\,\text{mm}$ $(L \times B \times H)$ steel plates. The excitation of this model is also point loading with magnitude $F = 1\,N$ at the co-ordinates $0{\cdot}2, 0{\cdot}25(0{\cdot}2, 0{\cdot}25)$ for the 1/3 octave band. For the first simulation of the second model, the two main parameters consist of $f_c = 3000$ Hz and $\eta = 0{\cdot}05$. Figures 13(a) and (b) show the energy density distributions of the displacement solution. The energy density decays more steeply in the direction of the x axis than the y axis because the reinforcing beams attenuate vibrational power transmission. Figures 14(a) and (b) show energy density distributions of the power flow solutions. At each junction, energy density discontinuities of 1–2 dB appear. Figures 15 and 16 show the intensity fields of the displacement solutions and power flow solutions, respectively.

For the following simulation for the second model, the center frequency, $f_c = 5000$ Hz and the internal loss factor, $\eta = 0{\cdot}15$ are increased. Figures 17(a) and (b), Figures 18(a) and (b) show the energy density distributions of the displacement solutions and the power

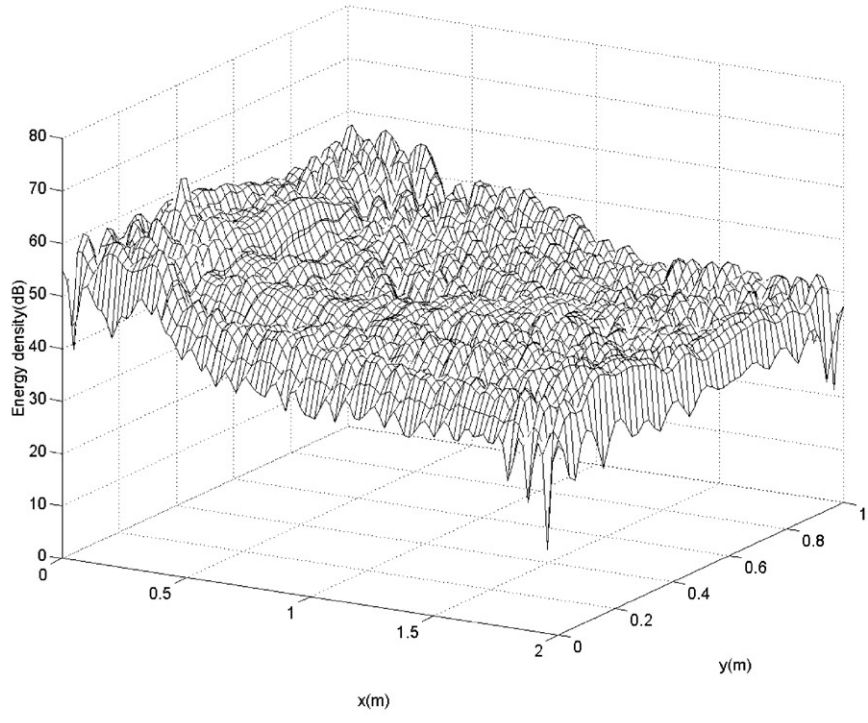

(a)

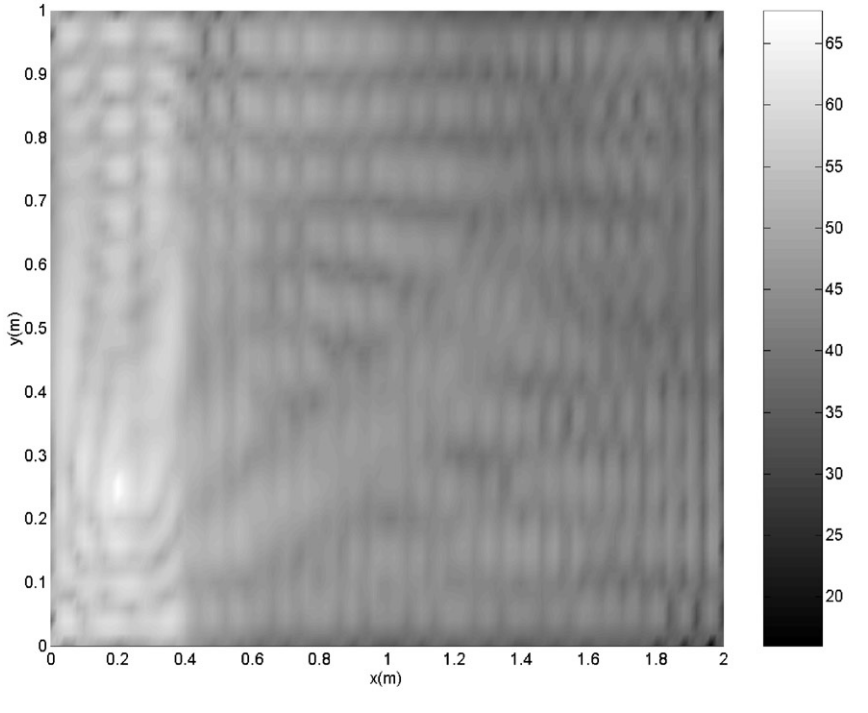

(b)

Figure 13. Energy density distributions of the displacement solutions when $f_c = 3000\,\text{Hz}$ and $\eta = 0{\cdot}05$. (a) 3-dimensional view; (b) 2-dimensional view.

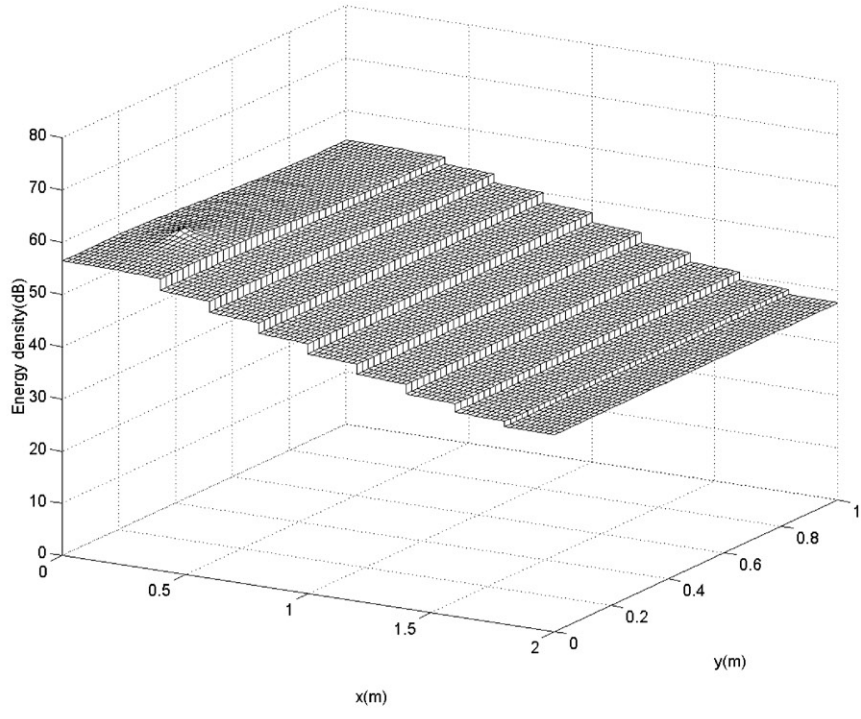

(a)

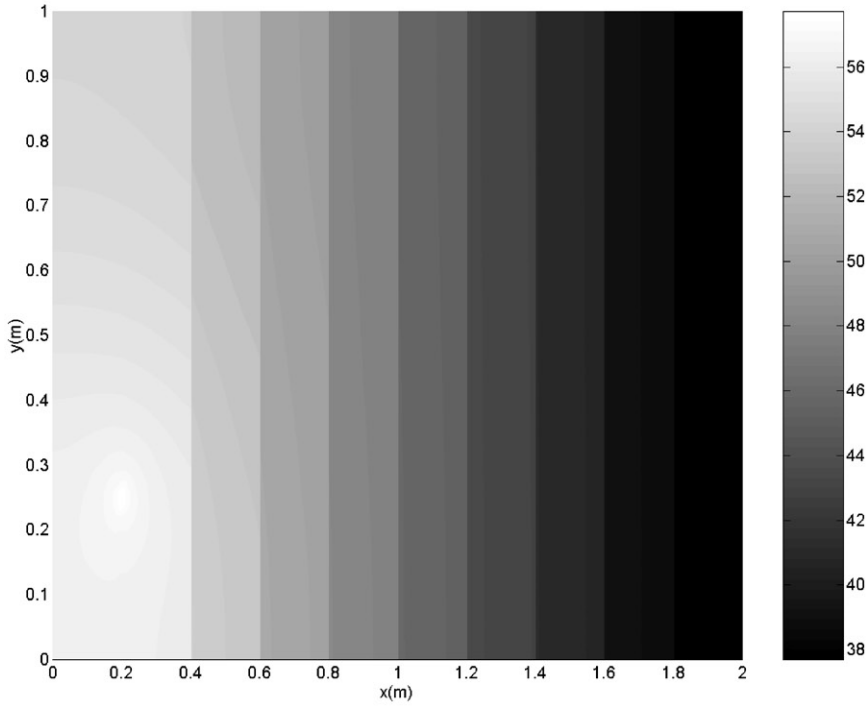

(b)

Figure 14. Energy density distributions of the power flow solutions when $f_c = 3000\,\text{Hz}$ and $\eta = 0{\cdot}05$. (a) 3-dimensional view; (b) 2-dimensional view.

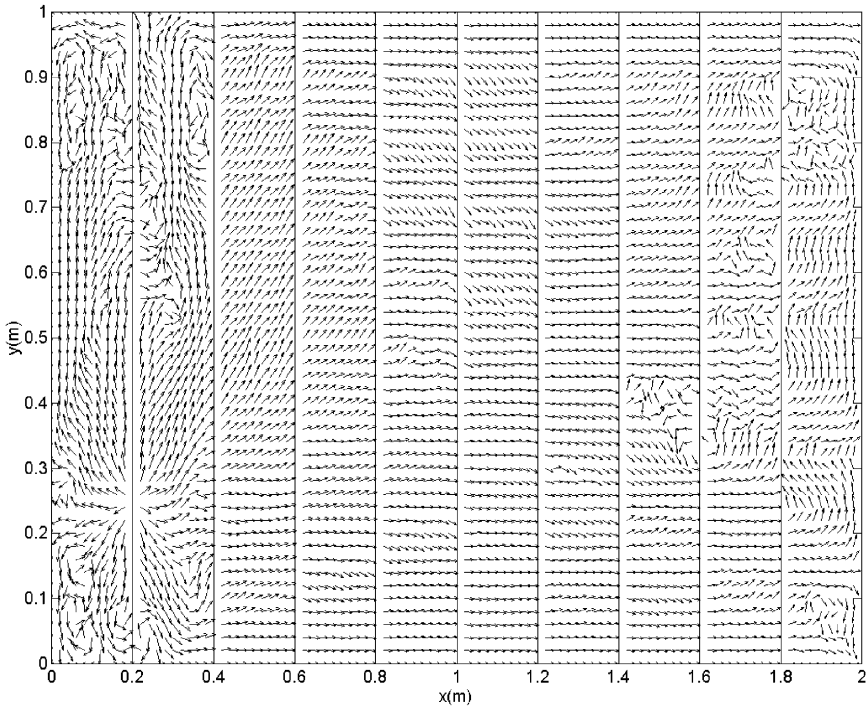

Figure 15. Intensity field of the displacement solutions when $f_c = 3000$ Hz and $\eta = 0{\cdot}05$.

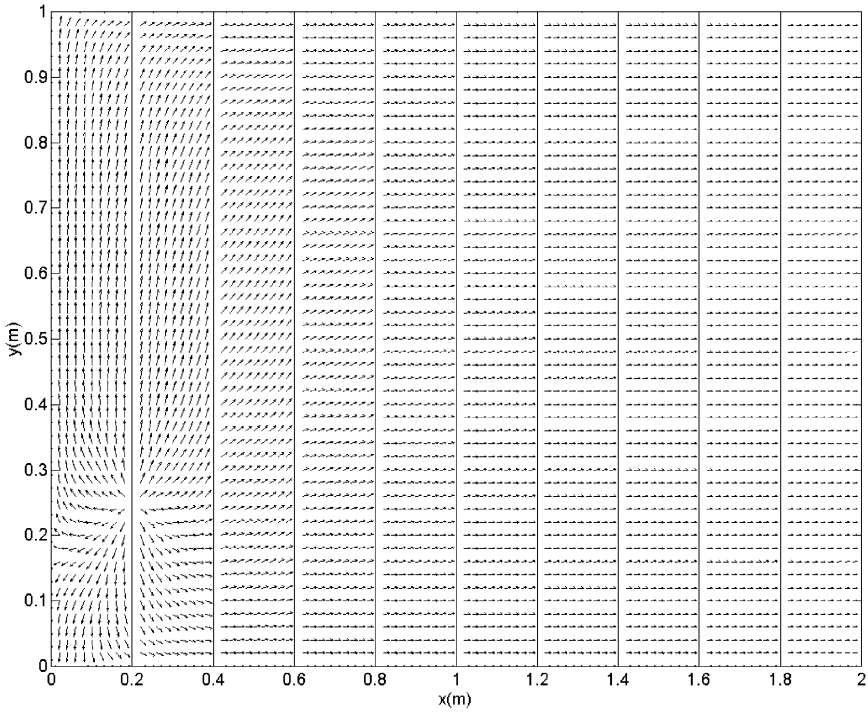

Figure 16. Intensity field of the power flow solutions when $f_c = 3000$ Hz and $\eta = 0{\cdot}05$.

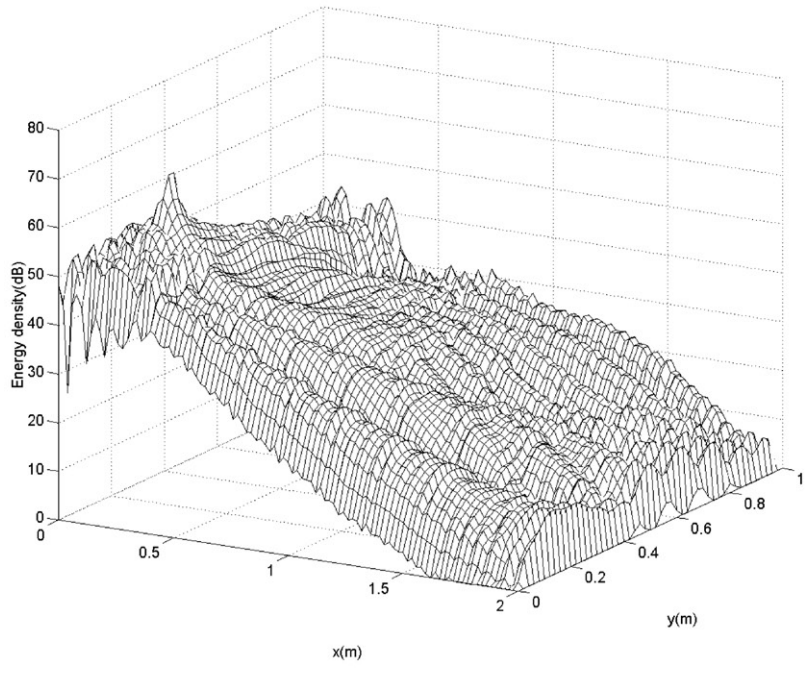

(a)

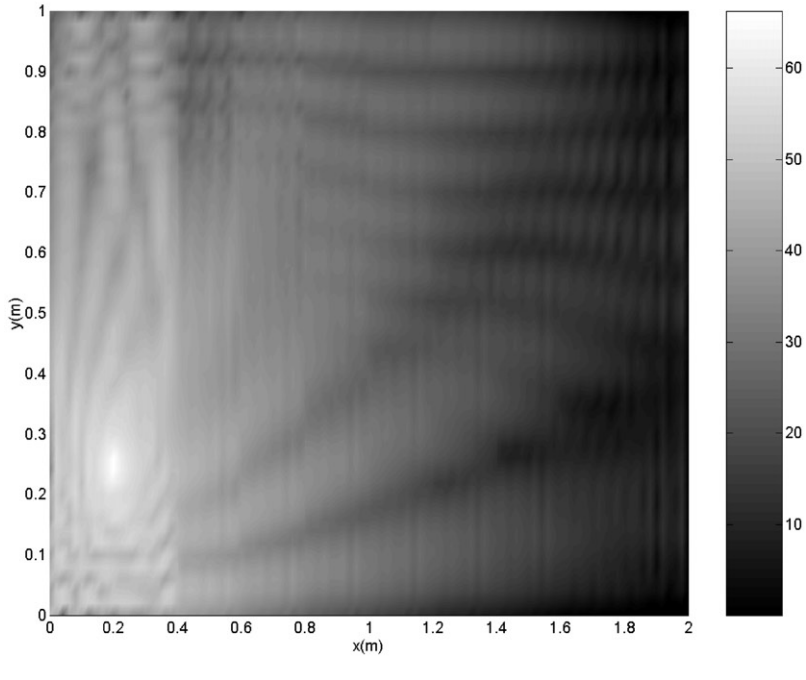

(b)

Figure 17. Energy density distributions of the displacement solutions when $f_c = 5000\,\text{Hz}$ and $\eta = 0{\cdot}15$. (a) 3-dimensional view; (b) 2-dimensional view.

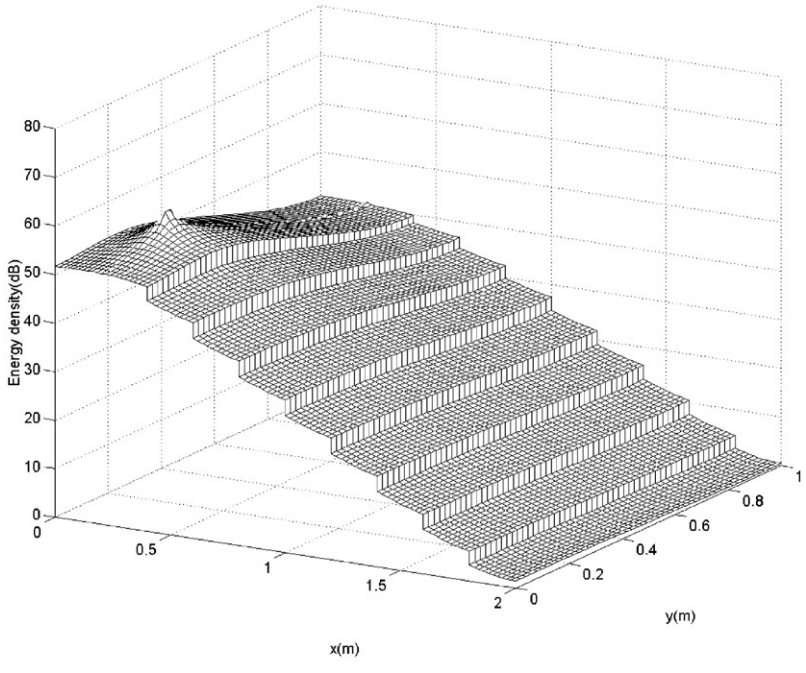

(a)

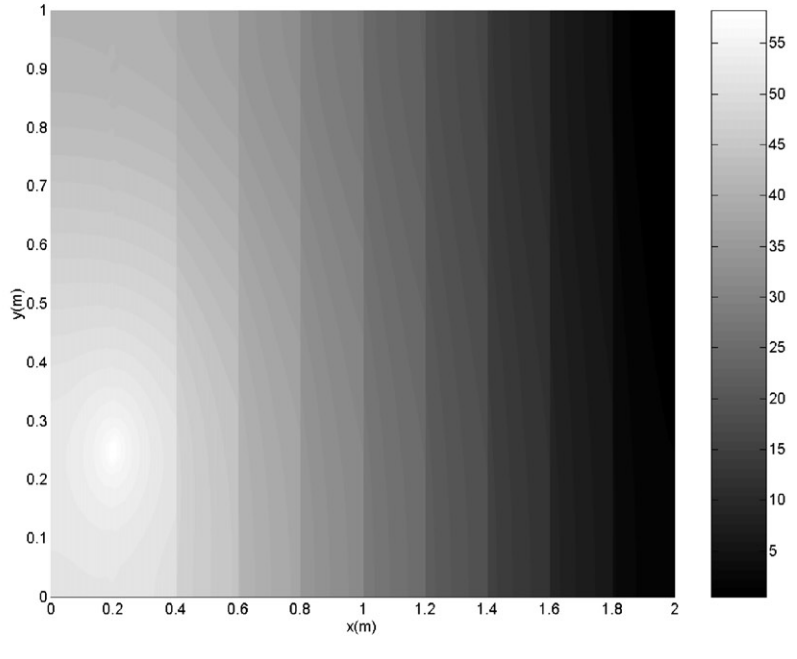

(b)

Figure 18. Energy density distributions of the power flow solutions when $f_c = 5000\,\text{Hz}$ and $\eta = 0{\cdot}15$. (a) 3-dimensional view; (b) 2-dimensional view.

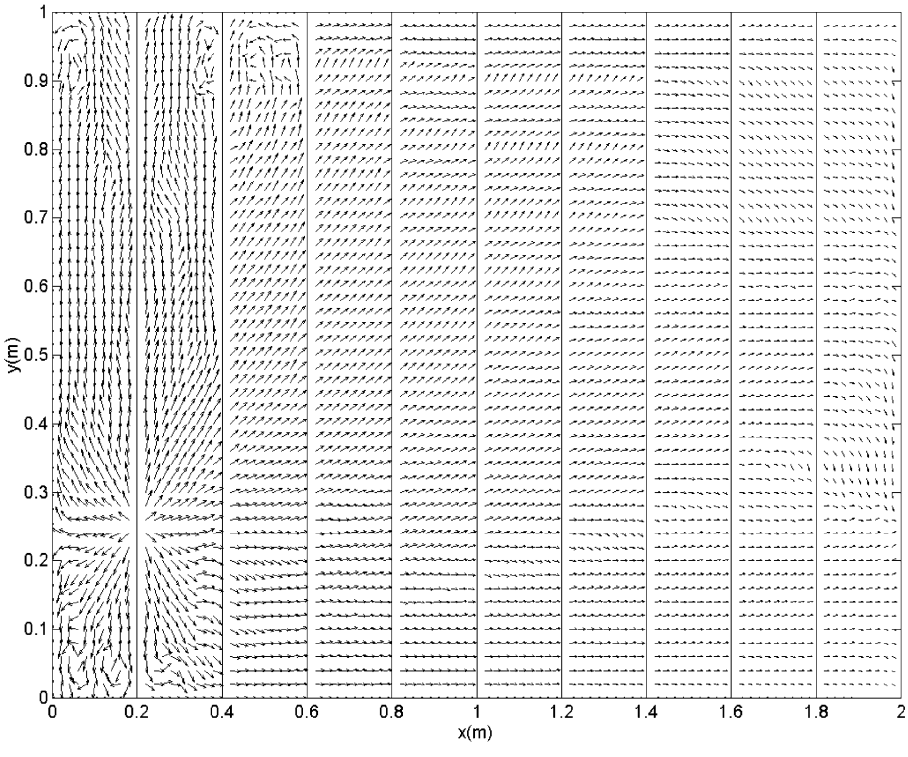

Figure 19. Intensity field of the displacement solutions when $f_c = 5000$ Hz and $\eta = 0{\cdot}15$.

flow solutions, respectively. Figures (19) and (20) show the intensity fields of the displacement solutions and the power flow solutions. For the multi-beam reinforced plate structures, the results of the power flow solutions also represent smooth and averaged results of the displacement solutions.

5. CONCLUSIONS

In this study, the power flow analysis method has been developed to predict the vibrational response of the reinforced beam–plate coupled structures in frequencies ranging from the medium to high. The energy density of the power flow solutions satisfies the energy governing equations in homogeneous plate domains. On the plate edges, the intensity of the power flow solutions is zero due to simple supports. On the beam–plate junctions, adequate power flow coupling relationships are applied to consider the reflected and transmitted power at the boundaries.

To verify the developed power flow analysis, numerical simulations for the two models were performed. As expected, the energy density of the power flow solutions decays smoothly in space and attenuates at the junctions, while the intensity of the power flow solutions spreads over the plates from the loading location. Compared with displacement solutions, power flow solutions exhibit good agreement with respect to the global decay and the attenuation patterns of the vibrational energy. It is concluded that power flow analysis can be an effective tool of vibration prediction for reinforced beam–plate coupled structures.

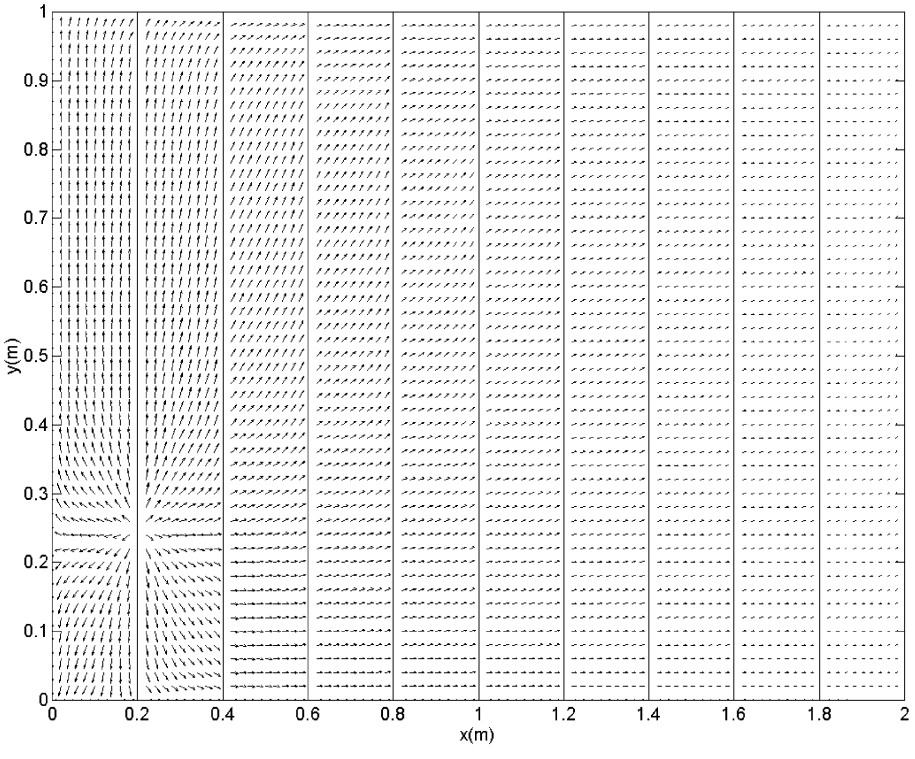

Figure 20. Intensity field of the power flow solutions when $f_c = 5000$ Hz and $\eta = 0{\cdot}15$.

REFERENCES

1. J. C. Wohlever and R. J. Bernhard 1992 *Journal of Sound and Vibration* **153**, 1–19. Mechanical energy flow models of rods and beams.
2. O. M. Bouthier and R. J. Bernhard 1992 *American Institute of Aeronautics and Astronautics Journal* **30**, 616–623. Models of space-averaged energetics of plates.
3. P. E. Cho 1993 *Ph.D. Thesis*. Energy flow analysis of coupled structures.
4. T. D. Sharton and R. H. Lyon 1968 *Journal of the acoustical society of America* **43**, 1332–1343. Power flow and energy sharing in random vibration.
5. D.-H. Park 1999 *M.S. Thesis, Seoul National University*. Vibration power flow analysis of coupled plates and box-type structures.
6. D.-H. Park, S.-Y. Hong, H.-G. Kil and J.-J. Jeon 2001 *Journal of Sound and Vibration* **244**, 651–668. Power flow model and analysis of in-plane waves in finite coupled thin plates.
7. S.-H. Seo 2000 *M.S Thesis, Seoul National University*. Power flow finite element method for the various plate structures in shape.
8. L. Cremer, M. Heckl and E. E. Ungar 1988 *Structure-borne Sound*. Berlin: Springer-Verlag; (second edition.)
9. R. S. Langley and K. H. Heron 1989 *Journal of Sound and Vibration* **143**, 241–253. Elastic wave tansmission through plate/beam junctions.
10. O. M. Bouthier and R. J. Bernhard 1995 *Journal of Sound and Vibration* **182**, 129–147. Simple models of energy flow in vibrating membranes.
11. J. H. Ferziger 1981 *Numerical Methods for Engineering Application*. New York: John Wiley & Sons.